Geophysical Journal (1988) **92,** 73–88

Lithospheric flexure and deformation-induced gravity changes: effect of elastic compressibility and gravitation on a multilayered, thick-plate model

Jiaxiang Zhang and Teng-fong Wong

Department of Earth and Space Sciences, State University of New York at Stony Brook, Stony Brook, N.Y. 11794-2100, *U.S.A.*

Accepted 1987 June 15. Received 1987 June 2; in original form 1986 November 10

SUMMARY

An approach is formulated by which the theoretical admittance can be evaluated for the flexure of a multi-layered elastic plate overlying an inviscid fluid. The multi-layered elastic and compressible plate is subjected to well-posed boundary conditions. Gravitational body force, elastic compressibility and elastic coupling at the interfaces with elastic modulus contrast are fully accounted for. The elastic field solution was obtained by the propagator matrix technique. The contribution to gravity change from local density perturbation within the compressible plate is also included. Our calculation shows that the density perturbation component is smaller than the Bouguer component by at least an order of magnitude over the compensated waveband. The thin-plate approximation can be used with an effective flexural rigidity evaluated from the thickness-averaged values of the elastic moduli. If there is significant elastic coupling between the crust and the mantle, the discrepancy between our results and the incompressible, thick-plate model can be quite appreciable due to the different isostatic compensation mechanisms operative within the crust. Preliminary calculations show that similar conclusions would apply to the response functions for the sub-surface loading case. Our technique can also be used to compute the stress distribution in a multilayered plate. The numerical results show that the stresses can be appreciably different from that in a homogeneous plate.

Key words: admittance, Bouguer, density perturbation, flexure, stress

1 INTRODUCTION

It is a well-known phenomenon that over mountain ranges the Bouguer gravity anomaly has an inverse correlation with the topography. The principle of isostasy was introduced to explain this phenomenon. Two main isostatic compensation models were proposed by Pratt (1855) and Airy (1855). Both models are local compensation models based on the assumption that above a certain 'depth of compensation' the masses of all columns are approximately equal. In these models the lithosphere is treated as a set of blocks floating on an inviscid fluid. No block can hold a neighbouring block either up or down by exerting a vertical traction on the side-walls. This implies that there are no vertical shear stresses within a continuous system in local isostatic equilibrium (Dahlen 1981).

A more realistic approach is to treat the lithosphere as an elastic plate. Surface loads cause flexure of the lithosphere and isostatic compensation then occurs on a regional scale. A powerful way to understand the compensation mechanism is to analyse theoretically the linear transfer function resulting from the flexural process (Dorman & Lewis 1970), and to compare the theoretical results with observations. Both the admittance and the isostatic response function have been used. The admittance is originally defined as the spectral ratio of the free air gravity anomaly to the bathymetry observed in an oceanic region (McKenzie & Bowin 1976). If the Bouguer gravity anomaly is used, then the spectral ratio is usually referred to as the isostatic response function (Dorman & Lewis 1970; Banks *et al.* 1977).

Banks *et al.* (1977) calculated the isostatic response function for the thin-plate model (Vening Meinesz 1941) assuming that the wavelength of the flexure is long compared with the thickness of the plate. This problem can be treated analytically, and most of the results can be parameterized in terms of the 'flexural rigidity' from which the 'effective elastic thickness' of the plate can be inferred.

A thick-plate model has to be considered when the flexure wavelength (λ) and the thickness of the plate (H) are of the same order or $\lambda \ll H$, i.e. except when $\lambda \gg H$. McKenzie & Bowin (1976) treated a 2-D, thick elastic plate model to obtain the theoretical admittance function. The plate was assumed to be incompressible for the sake of mathematical convenience. Comer (1983) later treated the 2-D, thick elastically-compressible plate model, neglecting body force in the solid. He obtained analytic expressions for all the elastic fields. Based on an incompressible model

identical to that of McKenzie & Bowin (1976), Wolf (1985) suggested that the neglect of the body force (such as in Comer's study) can result in physically unreasonable singularities in the solution as the product of the shear modulus and the wave number vanishes. Comer (1986) commented on the limitations of Wolf's (1985) conclusion, and suggested that an analysis taking into account both elastic compressibility and body force could be performed.

The gravity anomaly associated with any deformation within an elastic medium has two components (Savage 1984). One is the Bouguer component related to the mass transport caused by the vertical displacement at an interface between two layers of different densities, and the other component is due to the density perturbation within the plate caused by the elastic deformation. Although Banks *et al.* (1977) have discussed the contribution to gravity change from the density perturbation caused by lithosphere flexure, they neglected the density perturbation component in their final results. This is justified because of the approximate nature of the thin-plate model. McKenzie & Bowin (1976) assumed incompressibility, and hence density perturbation within the plate was neglected. Walsh (1982) suggested that the contribution to gravity from density perturbation can be significant for the plate flexure problem.

In this study a multilayered, elastic plate model is considered. The plate is compressible and can have any value of Poisson's ratio. Only 1-D, harmonic loading will be considered. The basic equations of equilibrium for the multilayered gravitating model were derived by Love (1911). In the analysis of the deformation field, we follow an approach similar to that of Cathles (1975) and Ward (1984) with a solution procedure based on the propagator matrix technique (Haskell 1953).

The general solutions for both the Bouguer component and the density perturbation component of the gravity change are obtained. We computed the theoretical admittance and isostatic response function as a function of wavelength. We analysed systematically the dependence of the compensation behaviour on the plate thickness, as well as on the density contrast and elastic mismatch of the layers. A preliminary analysis of the sub-surface loading problem and the stress distribution was also made.

2 FLEXURE OF A MULTILAYERED, ELASTIC PLATE

The problem that concerns us in this study is the flexure of the lithosphere whose thickness is much smaller than the radius of the Earth. Therefore the flat Earth model is considered. For the case that the density varies only in the z axis (pointing vertically downward), the governing equations for equilibrium in an elastic medium under hydrostatic pre-stress and constant uniform gravitation are (Love 1911; Cathles 1975):

$$\nabla \cdot \boldsymbol{\sigma} = \rho g \nabla \cdot \mathbf{U}\mathbf{e}_z - \rho g \nabla U_z \tag{1}$$

$$\nabla^2 \phi_1 = -4\pi G \nabla \cdot (\rho \mathbf{U}), \tag{2}$$

where ρ and g are the density and gravitational acceleration in the absence of the deformation, $\mathbf{U}$ is the displacement vector, $\boldsymbol{\sigma}$ is the stress perturbation tensor, ϕ_1 is the gravitational potential perturbation, G is the universal gravitational constant and $\mathbf{e}_z$ is a unit vector along the positive z-axis. The stress is related to the displacement gradient by Hooke's law. The first term on the right-hand side of equation (1) represents the body force perturbation due to dilatation, and the second term represents contribution from the hydrostatic pre-stress. Following previous studies (Cathles 1975; Ward 1984), we will assume constant gravitation, i.e. g is constant and hence the perturbation of body force (due to a term given by $\rho \nabla \phi_1$) should be of second order and is neglected in equation (1).

We will consider the deformation of a plate in a state of plane strain with a normal load $q \exp(ikx)$ applied at the top. If the density and elastic moduli are a function of z only, then the stress and displacement can be expressed as:

$$\begin{aligned} U_m(x, z) &= u_m(z) \exp(ikx) \\ \sigma_{mn}(x, z) &= \tau_{mn}(z) \exp(ikx). \end{aligned} \tag{3}$$

The indexes m and n can have values equal to x or z.

Substituting (3) into (1) and using Hooke's law, we have a set of four first-order differential equations:

$$\mathbf{V}'(z) = \mathbf{M}(k, z)\mathbf{V}(z), \tag{4}$$

where $\mathbf{V}'(z)$ is the derivative (with respect to z) of the solution column vector $\mathbf{V}(z)$:

$$\mathbf{V}(z) = (iu_x(z), u_z(z), i\tau_{zx}(z), \tau_{zz}(z))^T.$$

$\mathbf{M}(k, z)$ is a 4×4 matrix containing the depth-dependent elastic constants and densities (Appendix I).

For the case that the elastic moduli and density are constant between z and z_0, then $\mathbf{M}(k, z) = \mathbf{M}(k)$ and the general solution of (4) is:

$$\mathbf{V}(z) = \exp[\mathbf{M}(k)(z - z_0)]\mathbf{V}(z_0) = \mathbf{P}(k, z, z_0)\mathbf{V}(z_0). \tag{5}$$

Here $\mathbf{P}(k, z, z_0)$ is the propagator matrix which can be expressed as a polynomial of the matrix $\mathbf{M}(k)$ (Appendix I), the evaluation of which requires only a few matrix multiplications.

The elastic plate is composed of n layers at $0 < z < H$, and each layer is homogeneous and isotropic (Fig. 1). Within the jth layer of thickness h_j, the Poisson's ratio is v_j, the Young's modulus is E_j and the density is ρ_j. The elastic lithosphere floats on an inviscid fluid of density ρ_m and deforms due to a vertical load of thickness $l \exp(ikx)$ and density ρ_b on the top surface ($z = 0$), all being submerged beneath sea-water of density ρ_w in an oceanic region. The depth of seawater is d.

According to equation (5), we have:

$$\begin{aligned} &\mathbf{V}(z_{n-1}) = \mathbf{P}(k, z_{n-1}, H)\mathbf{V}(H) \\ &\mathbf{V}(z_{n-2}) = \mathbf{P}(k, z_{n-2}, z_{n-1})\mathbf{V}(z_{n-1}) \\ &\cdots \qquad\qquad \cdots \\ &\mathbf{V}(0) = \mathbf{P}(k, 0, z_1)\mathbf{V}(z_1). \end{aligned} \tag{6}$$

It is required that the displacement and traction be continuous across the solid–solid boundaries. Therefore we can relate the solution vector $\mathbf{V}(0)$ at the surface of the elastic lithosphere to $\mathbf{V}(H)$ at the bottom of the plate from (6):

$$\mathbf{V}(0) = \mathbf{P}_m \mathbf{V}(H), \tag{7}$$

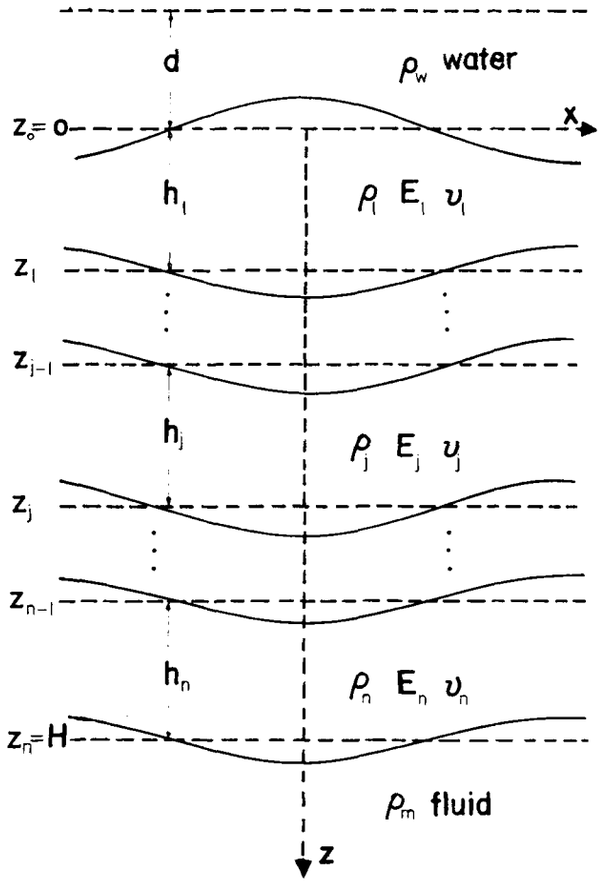

Figure 1. Sketch of a multilayered elastic plate floating on an inviscid fluid of density ρ_m with a harmonic load on its upper surface. All are submerged beneath sea-water of density ρ_w for an oceanic region and $\rho_w = 0$ for a continental region. υ_j, E_j, ρ_j and h_j ($j = 1, 2, \ldots, n$) are the Poisson's ratio, Young's modulus, density and thickness of jth layer, respectively.

where $\mathbf{P_m}$ is the product of the propagator matrices of the n layers, which depends on the material properties υ_j, E_j, ρ_j, the thicknesses h_j ($j = 1, 2, \ldots, n$) and the wave number k.

There are two vertical forces acting on the top of the plate: one is due to the loading material of the density ρ_b with thickness $l\exp(ikx)$ ($1 < 0$), another one is the buoyancy force from the sea-water acting on the loading material in the direction opposite to the first one. Hence:

$$\tau_{zz}(0) = \rho_b g l + \rho_w g \Delta, \tag{8}$$

where $\Delta = -(1 + u_z(0))$ is the topography at sea-floor. The minus sign arises because topography is measured positive upwards and z positive downwards.

At the bottom of the plate, the normal stress is equal to the buoyancy force from the fluid due to the vertical displacement:

$$\tau_{zz}(H) = -\rho_m g u_z(H). \tag{9}$$

Since no shear stress is applied on the top and the shear stress within a liquid layer vanishes, continuity of stress requires that:

$$\begin{aligned} \tau_{zx}(0) &= 0 \\ \tau_{zx}(H) &= 0 \end{aligned} \tag{10}$$

By substituting (8), (9) and (10) into (7), we obtain a set of four linear equations with four unknowns ($iu_x(0)$, $u_z(0)$, $iu_z(H)$ and $u_z(H)$) when the densities and elastic moduli of the elastic layers are given. We can solve for these four unknowns and hence $\mathbf{V}(0)$ and $\mathbf{V}(H)$ are determined. It is then easy to obtain $\mathbf{V}(z)$ ($0 < z < H$) through (6). By setting $\rho_w = 0$, we can also obtain the solution of the stress and displacement for a continental region.

The solution procedure for the elastic fields outlined above is identical to that of Cathles (1975) and the boundary conditions here are identical to Mckenzie & Bowin's (1976). We have checked that our results for the single-layer case ($n = 1$) with Poisson's ratio $\upsilon = 0.5$ agree with McKenzie & Bowin's (1976). Similarly, if we neglect body force ($g = 0$) in the elastic solid medium and set $\rho_w = 0$, then the results reduce to those of Comer (1983).

3. GRAVITY CHANGE AND TRANSFER FUNCTION DUE TO THE FLEXURE OF A THICK PLATE

The perturbation of the gravitational potential satisfies Laplace's equation in a free space and Poisson's equation (equation 2) in a region subjected to density perturbation. The solution can be expressed formally by Poisson's integral:

$$\phi_{1(\mathbf{x}')} = G \int_V \frac{\nabla \cdot (\rho \mathbf{U})}{R(\mathbf{x} - \mathbf{x}')} d\mathbf{x}, \tag{11}$$

where $R(\mathbf{x} - \mathbf{x}')$ is the distance between field point $\mathbf{x}'$ and source point $\mathbf{x}$. The volume integral is evaluated throughout the region experiencing density change.

The numerator of the integrand can be expressed as:

$$\nabla \cdot (\rho \mathbf{U}) = \rho'(z) U_z + \rho(z) \nabla \cdot \mathbf{U}, \tag{12}$$

where the first convective term represents the mass transport at an interface with density contrast (vertical density gradient $\rho'(z) \neq 0$) caused by the vertical displacement, and the second term is the local density perturbation due to elastic compressibility ($\nabla \cdot \mathbf{U} \neq 0$) at a fixed point in space. We will consider the two terms separately in the following analysis, and refer to the gravity change from the first term as the Bouguer component (δg^B) and the second one as the density perturbation component (δg^d). In general, any deformation-induced gravity change can be considered as the sum of these two components.

3.1 Bouguer component

The density distribution for our multilayered model is shown in Fig. 1.

The theoretical admittance for the Bouguer component (Z^B) is related to the Bouguer component of the gravity change (measured at the sea-surface: $z = -d$) and the surface topography Δ ($= -(1 + u_z(0))$) by the following relationship:

$$\delta g^B = Z^B \Delta \exp(ikx'). \tag{13}$$

We show in Appendix II that Z^B for our multilayered

model is given by:

$$Z^{B} = 2\pi G \exp(-kd)\Big\{(\rho_1 - \rho_w) + \Big[\sum_{j=1}^{n-1}(\rho_{j+1} - \rho_j)u_z(z_j)\exp(-kz_j) + (\rho_m - \rho_n)u_z(H)\exp(-kH)\Big]\Big/(1 + u_z(0))\Big\}. \quad (14)$$

The above is analogous to the result of Banks *et al.* (1977). For the continental situation, there is no contribution from the sea-water and hence ρ_w and d can be set to zero. If we are only interested in the Bouguer gravity anomaly, the topographical contribution given by $2\pi G\rho_1\Delta$ has to be subtracted from equation (13). Consequently, the isostatic response function for the continental case is given by:

$$Q^{B} = 2\pi G\Big[\sum_{j=1}^{n-1}(\rho_{j+1} - \rho_j)u_z(z_j)\exp(-kz_j) + (\rho_m - \rho_n)u_z(H)\exp(-kH)\Big]\Big/(1 + u_z(0)). \quad (15)$$

3.2. Density perturbation component

Except for some preliminary results for a homogeneous elastic half-space obtained by Farrell (1972) and Walsh (1982), and for point-loading in an elastic–gravitational plate overlying a fluid–gravitational half-space by Rundle (1982, 1983), we are not aware of any analysis of the density perturbation component of the gravity change for the plate flexure problem. It is therefore useful to outline our theoretical results in a systematic manner. We will first treat the case with $g = 0$ in the solid and then generalize the result to the case with a constant g in the solid.

3.2.1 The case $g = 0$ in the solid

From equations (11) and (12), the contribution to the gravitational potential from density perturbation within the jth layer is:

$$\phi_j^d(\mathbf{x}') = G\rho_j \int_{v_j} \frac{\nabla\cdot\mathbf{U}}{R(\mathbf{x}-\mathbf{x}')}\,d\mathbf{x}, \quad (16)$$

where the volume integral is taken throughout the jth layer. Using Green's theorem, it can be shown that if a function can be expressed as the Laplacian of another function, e.g. $f(\mathbf{x}) = \nabla^2 F(\mathbf{x})$, the volume integral below can be simplified to a surface integral in the following manner:

$$\int_V \frac{f(\mathbf{x})}{R(\mathbf{x}-\mathbf{x}')}\,d\mathbf{x} = \int_s \Big[\frac{1}{R}\frac{\partial F}{\partial n} - F\frac{\partial}{\partial n}\Big(\frac{1}{R}\Big)\Big]\,ds \quad (17)$$

with $\mathbf{x} \neq \mathbf{x}'$ so that $\nabla^2(1/R) = 0$. Here n is the outward unit normal vector of the surface s which encloses the volume V.

For this case, we can obtain the following simple relation (see Appendix I, (I-11)) for the local dilatation:

$$\nabla\cdot\mathbf{U} = [(1-2v)/k]\nabla^2[iu_x\exp(ikx)]. \quad (18)$$

Since the field point $\mathbf{x}'$ is in free space, we can use equation (17). By substituting (18) into (16), and using Green's theorem, we obtain:

$$\phi_j^d = \frac{G(1-2v_j)\rho_j}{k}\int_{-\infty}^{+\infty}\Big[-\frac{iu_x'(z_{j-1})}{R_{j-1}} + \frac{(z'-z_{j-1})iu_x(z_{j-1})}{R_{j-1}^{3/2}} + \frac{iu_x'(z_j)}{R_j} - \frac{(z'-z_j)iu_x(z_j)}{R_j^{3/2}}\Big]\exp(ikx)\,dx\,dy, \quad (19)$$

where $R_j = [(x'-x)^2 + (y'-y)^2 + (z'-z_j)^2]^{1/2}$.

The integral in equation (19) can be differentiated to obtain the vertical component of the gravity change at $\mathbf{x}'$ which has a closed form as follows:

$$\delta g_j^d = -\partial\phi_j^d/\partial z' = \frac{2\pi G\rho_j(1-2v_j)}{k}\exp(kz')\exp(ikx')\{[iu_x'(z_{j-1}) + iku_x(z_{j-1})]\exp(-kz_{j-1}) - [iu_x'(z_j) + iku_x(z_j)]\exp(-kz_j)\} \quad (20)$$

From equation (4) we know that $iu_x'(z)$ $(z_{j-1} \leq z \leq z_j)$ is the first element of vector $\mathbf{M_j V}(z)$ and $iu_x(z)$ is the first element of vector $\mathbf{V}(z)$. Therefore, we can write (20) in the following form:

$$\delta g_j^d = \frac{2\pi G\rho_j(1-2v_j)}{k}W_j^1\exp(kz')\exp(ikx') \quad (21)$$

where W_j^1 is the first element of vector $\mathbf{W}_j$ given by:

$$\mathbf{W_j} = (\mathbf{M_j} + k\mathbf{I})[\mathbf{V}(z_{j-1})\exp(-kz_{j-1}) - \mathbf{V}(z_j)\exp(-kz_j)] \quad (22)$$

and $\mathbf{I}$ is the identity matrix.

The total gravity change δg^d due to the density perturbation from all the elastic layers is found by summing (21) over all j:

$$\delta g^d = Z^d\Delta\exp(ikx') = \frac{2\pi G\exp(kz')\exp(ikx')}{k}\sum_{j=1}^{n}\rho_j(1-2v_j)W_j^1 \quad (23)$$

where Z^d is the theoretical admittance corresponding to the density perturbation component, and Δ is the surface topography given by $-(1 + u_z(0))$.

3.2.2. Plate subjected to constant gravitation

For the plate with a constant g, we obtain the following relation through (I-9) of Appendix I:

$$\nabla\cdot\mathbf{U} = \frac{(1-v)E^2}{2[\rho g k(1+v)]^2(1-2v)}\nabla^4[(iku_x + u_z')\exp(ikx)]. \quad (24)$$

Using equation (17) and the above expression for the local dilatation, the volume integral in equation (16) can again be reduced to a surface integral. The integrand of the surface integral for this case involves $\nabla^2[(iku_x + u_z')\exp(ikx)]$, and after a considerable amount of algebra, we obtained explicit expressions for the density perturbation component of the potential. By differentiating the potential, we obtain the following results for the density perturbation

component of gravity change:

$$\delta g^d = Z^d \Delta \exp(ikx')$$

and

$$Z^d = \frac{-2\pi G \exp(kz')}{(1+u_z(0))(gk)^2} \sum_{j=1}^{n} \frac{(1-v_j)E_j^2}{2\rho_j(1+v_j)^2(1-2v_j)} \times (kA_j^1 + B_j^2), \quad (25)$$

where A_j^1 is the first element of vector $\mathbf{A_j}$ and B_j^2 is the second element of vector $\mathbf{B_j}$ in which;

$$\mathbf{A_j} = (\mathbf{M_j} - k\mathbf{I})(\mathbf{M_j} + k\mathbf{I})^2[\mathbf{V}(z_{j-1}) \exp(-kz_{j-1}) - \mathbf{V}(z_j) \exp(-kz_j)] \quad (26)$$

$$\mathbf{B_j} = \mathbf{M_j}\mathbf{A_j}$$

and Z^d is the theoretical transfer function corresponding to density perturbation component for the case with a constant g in the solid.

When the admittance is considered, we will set $z' = -d$ (at sea-surface) with density of seawater ρ_w for (23) and (25). The isostatic response function corresponds to $z' = 0$, and $\rho_w = 0$.

4 NUMERICAL EXAMPLES AND DISCUSSION

4.1 Comparison with the incompressible thick plate model

A common model used to interpret quantitatively the tectonic implications of observed gravity, bathymetry and admittance has been that of McKenzie & Bowin (1976) as modified by Watts (1978). It has been applied in the analysis of isostasy in sea-mount chains (Watts 1978; Cazenave & Dominh 1984), mid-ocean ridges (Cochran 1979; Kogan & Kostoglodov 1981; Tamsett 1984) and aseismic ridges (Detrick & Watts 1979). This model considers a three-layered plate overlying an inviscid fluid. The top two layers have densities and thicknesses comparable to those of layers 2 and 3 of an oceanic crust, whereas the third layer has density and elastic properties representative of the upper mantle. The theoretical admittance is given by:

$$Z(k) = 2\pi G(\rho_2 - \rho_w) \exp(-kd)[1 - [(\rho_3 - \rho_2) \exp(-kt_2) + (\rho_m - \rho_3) \exp(-kt_c)]/[(\rho_m - \rho_2) + 4(\rho_m - \rho_w)Mk^2h^2AB^{-1}]], \quad (27)$$

where t_2 is the thickness of layer 2; t_c is the mean thickness of the crust; ρ_3 is the density of layer 3; ρ_w is the density of the sea-water; ρ_m is the density of the upper mantle; $M = E/3gh(\rho_m - \rho_w)$, where E is Young's modulus and the thickness of the upper mantle is $2h$; $A = [(\sinh 2kh)/2kh]^2 - 1$; and $B = [(\sinh 4kh)/4kh]^2 + 1$.

One assumes in the derivation of the above expression that the two crustal layers are in local isostatic equilibrium by a mechanism such as Airy's. The third layer in the upper mantle is elastic and incompressible, and isostatic compensation is regional via flexure of this sub-crustal layer. In the quantitative analysis of observed admittances, the thicknesses and densities of the top two layers are inferred from seismic and core data. The Young's modulus of the third layer is usually assigned a value comparable with that inferred from seismic data. The thickness of the third layer in the upper mantle is not fixed *a priori*—it is a free parameter to be estimated by comparison of the observations with the theoretical admittances corresponding to various thickness values. The thickness so determined for the sub-crustal layer is usually referred to as the 'elastic thickness'.

This approach assumes that the rheological properties and mechanical response are such that the oceanic crust and the upper mantle have drastically different isostatic compensation mechanisms. It has been suggested (McKenzie & Bowin 1976) that the oceanic crust (especially at localities close to the ridge axis) is not elastic because it is broken by faults and probably undergoing metamorphism. However, rock mechanics studies indicate that crustal rocks, even in a highly fractured state, would have appreciable mechanical strength and elasticity (Byerlee 1978; Goetze & Evans 1979).

We decided to investigate the effect of mechanical coupling between the crust and the mantle on the flexural behaviour. For comparison with Watts' (1978) model, we also considered a three-layered plate as shown in Fig. 2, the physical parameters for which are compiled in Table 1. We have assigned representative elastic modulus values as

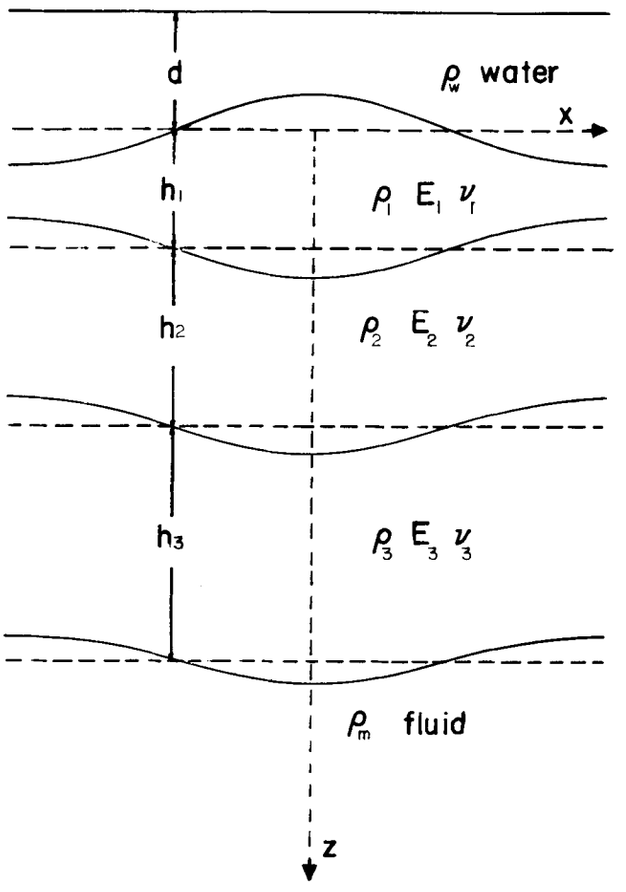

Figure 2. Sketch of a three-layered model used to calculate the admittance Z and isostatic response function Q. The parameters are shown in Table 1.

Table 1. Parameters of Fig. 2. Depth of seawater $d = 5$ km, density of seawater $\rho_w = 1030\,\mathrm{kg\,m^{-3}}$ and density of the inviscid fluid $\rho_m = 3400\,\mathrm{kg\,m^{-3}}$

The jth layer	first	second	third
Young's modulus E_j (GPa)	50	80	100
Poisson's ratio υ_j	0.25	0.28	0.36
Density ρ_j ($10^3\,\mathrm{kg\,m^{-3}}$)	2.6	2.9	3.4
Thickness h_j (km)	2	3	5–50

inferred from seismic data to the three layers (Birch 1966; Christensen 1982).

Our numerical results for the theoretical admittance using the full theory are shown by the solid lines in Fig. 3. For very short wavelengths, the theoretical admittance we calculated approaches the uncompensated admittance $2\pi G(\rho_b - \rho_w)\exp(-kd)$ which is solely due to the water-rock density contrast at the sea-floor. As the wavelength increases, the admittance begins to deviate from the uncompensated value, indicating the onset of regional compensation by plate flexure. For relatively long wavelengths, the admittance approaches that due to Airy's mechanism. Our computations show that the wavelength for the onset of regional compensation increases as a function of plate thickness.

There is appreciable discrepancy between the theoretical admittance we calculated and that from equation (27) (dashed lines in Fig. 3) for thicknesses of the sub-crustal layer ranging up to 45 km. The implication of such a discrepancy on data interpretation can be clarified referring to Detrick & Watts' (1979) data for the western Walvis Ridge (Fig. 4a) and Watts' (1978) data for the Hawaiian-Emperor seamount chain (Fig. 4b). The dashed lines in these figures are best-fit theoretical admittances

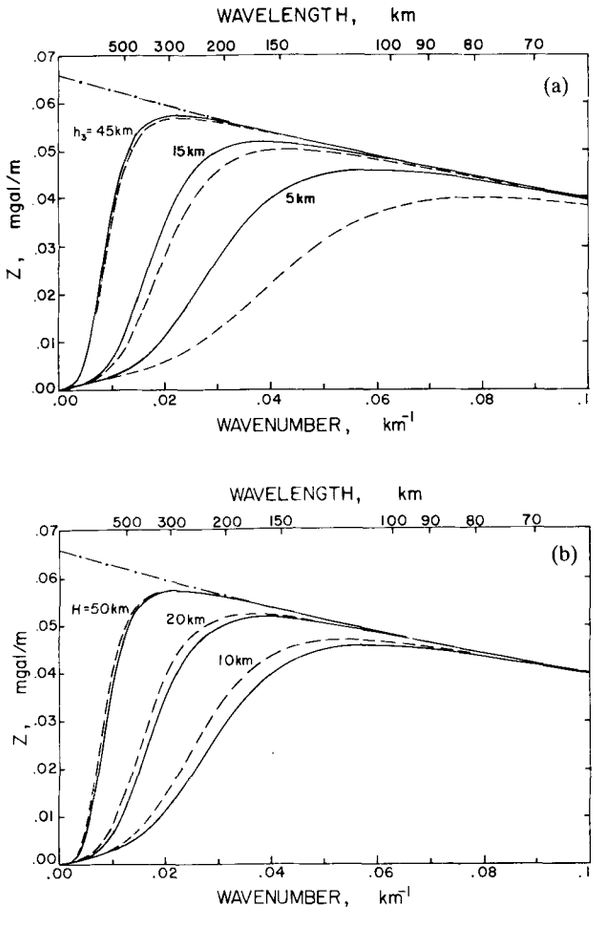

Figure 3. Theoretical admittances calculated from the full theory (solid lines) and incompressible plate model with equation (27) (dashed lines) for a three-layered plate as shown in Fig. 2 with parameters compiled in Table 1. The elastic moduli of the top two layers are not accounted for by the incompressible plate model. The chain line is the uncompensated admittance $2\pi G(\rho_b - \rho_w)\exp(-kd)$. (a) The admittances plotted with the thickness of the third layer vary from 5 to 45 km. (b) The admittances plotted with the elastic thickness of the plate varying from 10 to 50 km which are the sum of the thicknesses of the three layers (full theory) or just that of the sub-crustal layer (incompressible plate model).

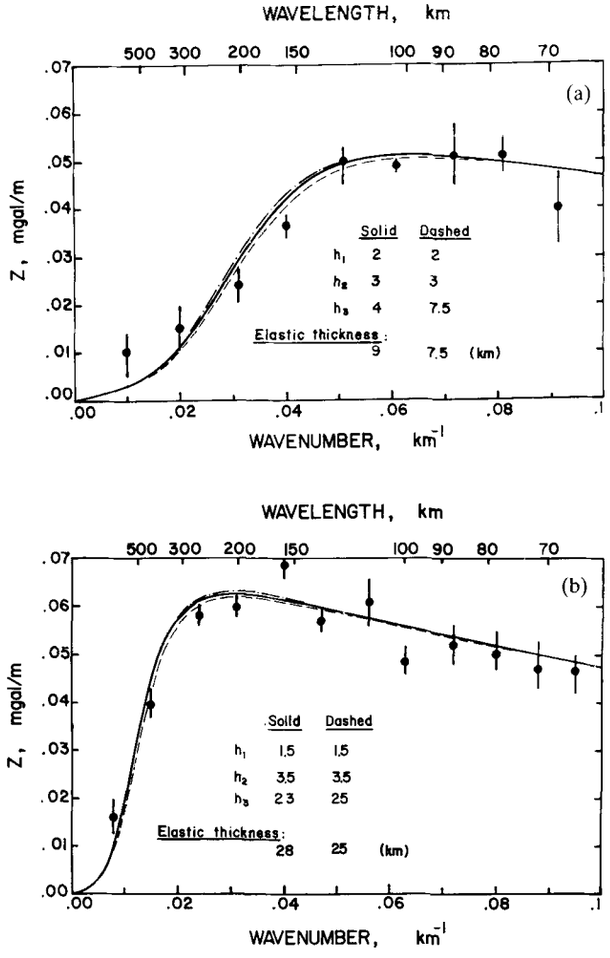

Figure 4. Observed admittance data (solid circles) and those from theoretical models: multilayerd model (solid line), incompressible plate model (dashed line) and thin-plate model (chain lines). (a) Observed data from the western Walvis Ridge (Detrick & Watts 1979). The parameters used to calculate the theoretical admittances are similar to Table 1 except that $d = 4$ km, $\rho_1 = 2700\,\mathrm{kg\,m^{-3}}$. (b) Observed data from the Hawaiian-Emperor sea-mount chain (Watts 1978). The parameters used to calculate the theoretical admittances are similar to Table 1 except that $d = 4.5$ km, $h_1 = 1.5$ km, $h_2 = 3.5$ km and $\rho_1 = 2800\,\mathrm{kg\,m^{-3}}$.

from the original references calculated using equation (27). Our computation in solid lines shows that almost identical admittance curves can be obtained with our model if a relatively thin sub-crustal layer is used. If elastic coupling is significant, a mechanical lithosphere extending 4 km (at western Walvis ridge) and 23 km (along the Hawaiian-Emperor sea-mount chain) into the upper mantle are implied by the observed admittances. If the crustal layers are decoupled from the upper mantle with local isostatic equilibrium within the crust, then the mechanical lithosphere is expected to extend further into the upper mantle (7.5 and 25 km, respectively.)

It should be kept in mind that since the crust and the upper mantle are mechanically coupled in our model, the elastic thickness is the sum of the thicknesses of the three layers (Fig. 3b) whereas the elastic thickness for Watts' (1978) model is just that of the sub-crustal layer. In other words, the elastic thicknesses implied by our theoretical admittances are 9 km (Fig. 4a) and 28 km (Fig. 4b) respectively.

Our parametric study indicates that the following general statement can be made: if elastic coupling among the crustal layers and the upper mantle is significant, then McKenzie & Bowin's (1976) model as modified by Watts (1978) will underestimate the elastic thickness, and at the same time it overestimates the extent of the mechanical lithosphere in the upper mantle. The discrepancy can be up to 5 km (the crustal thickness) for the three-layered plate model. Probably this is still within the reported uncertainties associated with elastic thickness values so estimated, although it is possible that such a systematic underestimation of the elastic thickness may bias the quantitative interpretation of the mechanical thickness versus age relation (Watts *et al.* 1980; McNutt 1984).

It is not easy to explain the discrepancy further on a rigorous mechanical basis. The stress distribution for a situation corresponding to equation (27) cannot be specified easily. Although a local isostatic mechanism such as Airy's apparently only requires vertical forces to balance, the true stable position of the crust equilibrates the vertical forces, horizontal forces and all moments locally at all points. Local isostasy over all wavelengths necessarily would require an unrealistically anisotropic mechanical response (McKenzie 1977; McNutt 1980; Dahlen 1981) and a highly heterogeneous stress distribution (Artyushkov 1973). Our model is based on a complete elasticity theory with well-posed boundary conditions. However, it involves a number of physical processes (including gravitational body force, elastic compressibility and elastic coupling among layers) the individual contribution of which is hard to sort out. We attempt to address this question in the next section.

4.2 Effect of elastic compressibility and gravitational body force on isostatic response function

Kogan & Kostoglodov (1981) gave an analytic expression for the theoretical admittance allowing for the compressibility of the elastic plate and the action of body force. Their biharmonic function approach is analogous to that of McKenzie (1976). However, we show in Appendix I that a biharmonic function can be found only if either the body force in the solid is neglected or the elastic medium is incompressible. Strictly speaking, Kogan & Kostoglodov's (1981) solution does not satisfy the equilibrium conditions for an elastic plate with body force included. Furthermore, they did not include the density perturbation component in their final solution of gravity anomaly.

It is more convenient in the following discussion to focus on only that part of the gravity anomaly which is directly related to isostatic compensation by the flexure process. In this sense, the isostatic response function Q (Dorman & Lewis 1970; Banks *et al.* 1977) is more suitable because the gravitational attraction due to both the topography and the water-rock interface has been removed.

The computations shown in Fig. 5 are all for the three-layered plate with physical parameters as specified in Table 1. The isostatic response functions for three elastic thicknesses (10, 30 and 55 km) are shown in Fig. 5(a). Typically the response function vanishes for short wavelengths over which the topography is uncompensated. As wavelength increases, Q decreases with the onset of

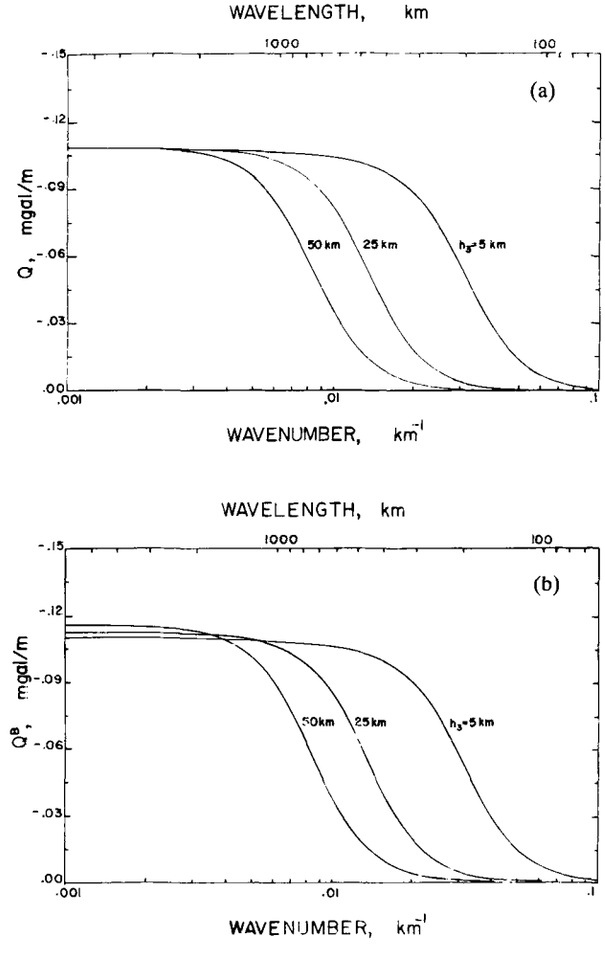

Figure 5. Isostatic response functions based on the three-layered model shown in Fig. 2 with $d = 0$, $\rho_w = 0$. The thickness of the third layer varies from 5 to 50 km. (a) Isostatic response function which is the sum of the Bouguer component Q^B and density perturbation component Q^d. (b) Bouguer component Q^B. (c) Density perturbation component Q^d. (d) The absolute value of the ratio Q^d/Q^B.

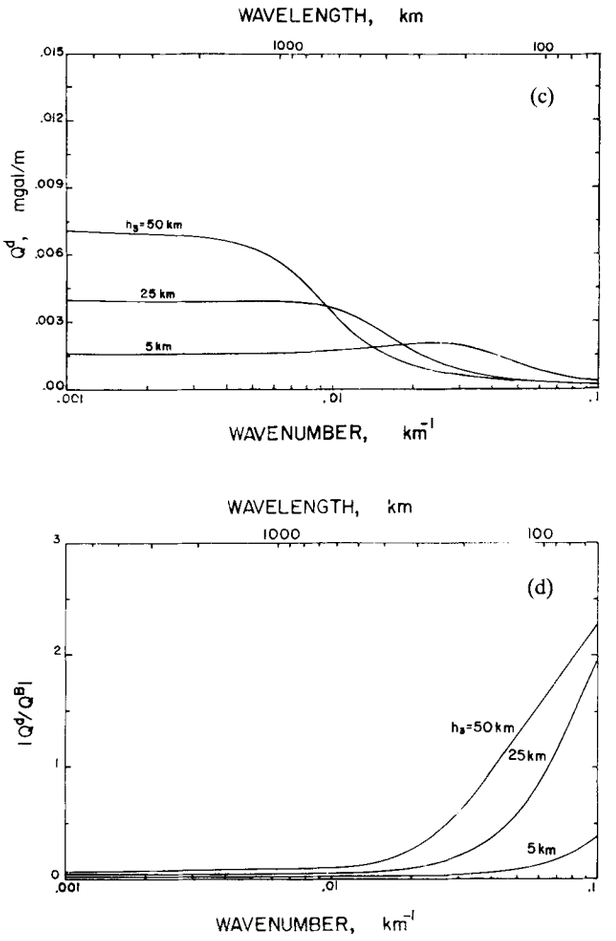

Figure 5. (c) and (d) (see previous page).

regional compensation, ultimately attaining a value given by $-2\pi G\rho_b$ for very long wavelengths corresponding to local compensation by Airy's mechanism.

The individual contributions for the Bouguer component (equation 15) and the density perturbation component (equation 25) are shown in Fig. 5(b) and (c) respectively. In general, the two components have opposite signs. Localized compression in the vicinity of the topography results in an increase in density and consequently an enhancement of gravity. The ratio of the two components is plotted in Fig. 5(d). At wavelengths for which isostatic compensation is appreciable, the density perturbation component is smaller than the Bouguer component by at least an order of magnitude and hence is negligible. Therefore the omission of this term in previous models does not introduce significant error into the interpretation of measurements of admittance or isostatic response function.

Recent theoretical analyses have shown that the density perturbation component can be significant for certain tectonic processes (Savage 1984). Numerical computation by Rundle (1978) (which was then confirmed by the analytic results of Walsh & Rice 1979) showed that the density perturbation component for a dilatational source in an elastic half-space should exactly cancel the Bouguer component. This conclusion is now routinely used in the quantitative interpretation of gravity anomaly associated with volcanic activity (e.g. Jachens & Eaton 1980; Jachens & Roberts 1985). In contrast, our numerical results show that the density perturbation component for the flexure process is negligible except within the uncompensated waveband for which the results approach the half-space solution (Farrell 1972; Walsh 1982; Rundle 1982).

The effect of gravitational body force on the isostatic response function is illustrated in Fig. 6(a) and (b). Again the computations are for a three-layered plate with physical parameters as specified in Table 1. For comparison, we have also computed the Bouguer component (Fig. 6a) and the density perturbation component (Fig. 6b) of the isostatic response function for the case with $g = 0$ in the solid medium, as shown in dashed lines. The solid lines are for the case with the plates subjected to constant gravitation. It can be seen from Fig. 6(a) that the Bouguer component is basically the same whether the gravitational body force is included or not. A small difference can be detected only for wavelengths beyond several thousands of kilometres.

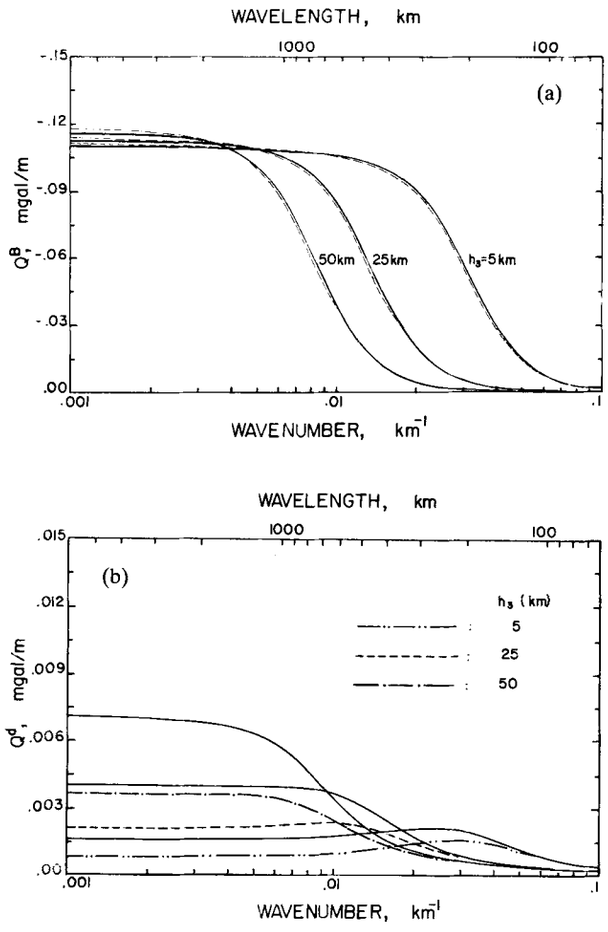

Figure 6. Illustration of the effect of gravitational body force on the isostatic response function: (a) Bouguer component Q^B and (b) Density perturbation component Q^d. The solid lines in (a) and (b) are calculated with the body force included. The dashed and chain lines in (a) and (b) are obtained by ignoring the body force in the solid. The computations are for a three-layered model (Fig. 2) with $d = 0$ and $\rho_w = 0$.

Figure 6(b) shows that the density perturbation component by itself can have quite different values corresponding to the constant gravitation and non-gravitation in the solid. The effect of the body force seems to be important over a broad range of wavelengths. This is not surprising in light of the recent observation by Ward (1984) that the stress field with a gravitational body force included can be significantly different from that of a plate not subject to body force. Since the density perturbation component of the isostatic response function is related to the trace of the stress tensor, one should expect the density perturbation component to be also sensitive to body forces.

However, since the contribution from the density perturbation component to the total gravity anomaly is negligible within the 'compensated' waveband (Fig. 5d), the omission of body force (such as in the 'thin plate' approximation and in Comer's study (1983)) is not expected to introduce significant error in the interpretation of observed isostatic response functions or admittances.

In summary, both the density perturbation component of the gravity change and the body force contribution can be neglected without serious consequences for the interpretation of the isostatic response function or the admittance. This implies that the discrepancy (Figs 3 and 4) between our computations using the full theory and the theoretical admittances calculated for the thick, incompressible plate model (equation 27) is principally due to differences in the boundary conditions at the Moho and in the isostatic compensation mechanism operative within the crust.

4.3 Comparison with the thin-plate model

Another common model to interpret the spectral data of gravity and bathymetry or topography is the thin-plate model (e.g. Walcott 1970; Banks *et al.* 1977; McNutt 1979). If the density structure within an elastic plate is that shown in Fig. 1, but the plate is elastically homogeneous, which is required in the thin-plate approximation, the theoretical admittances can be calculated thus:

$$Z(k) = 2\pi G \exp(-kd)\left\{(\rho_b - \rho_w) - \frac{(\rho_b - \rho_w)}{(\rho_m - \rho_b)} \times \left[1 + \frac{Dk^4}{g(\rho_m - \rho_b)}\right]^{-1}\left[\sum_{j=1}^{n-1}(\rho_{j+1} - \rho_j)\exp(-kz_j) + (\rho_m - \rho_n)\exp(-kH)\right]\right\}, \quad (28)$$

where ρ_w, ρ_b and ρ_m are the densities of sea water, loading material and inviscid fluid respectively; ρ_j is the density of the j-th layer ($j = 1, 2, 3, \ldots, n$); H is the elastic thickness which is the sum of the thicknesses of the n layer, and D is the flexural rigidity. If the plate is continuous, homogeneous and elastic, then the flexural rigidity D can be expressed unambiguously in terms of the plate thickness and elastic moduli:

$$D = EH^3/12(1 - v^2),$$

where E is Young's modulus, v is Poisson's ratio and H is the 'elastic thickness'. Elastic compressibility is accounted for in the thin-plate approximation, although the density perturbation component of the gravity change is usually neglected (Banks *et al.* 1977) and gravitational body force is not considered. Young & Hill (1986) gave a theoretical admittance (equation 10 in their paper) for a three-layered model which, except for a typographical error, is identical to equation (28) for the case $n = 3$. If there is elastic heterogeneity within the plate, it has never been very clear how the flexural rigidity should be interpreted. One may conjecture that there exists a homogeneous elastic plate whose flexural response is similar to that of the heterogeneous elastic plate as a whole, and the effective elastic moduli have values somewhere between the lowest and highest elastic moduli of the heterogeneous plate. When the elastic modulus contrast within our three-layered plate model is comparable with that inferred from seismic data with representative values such as in Table 1, by comparing our numerical results using the full theory with theoretical admittances obtained from the thin-plate approximation equation (28), with $n = 3$, we have established empirically that the thin-plate model is a reasonable approximation if the flexural rigidity is calculated using the following

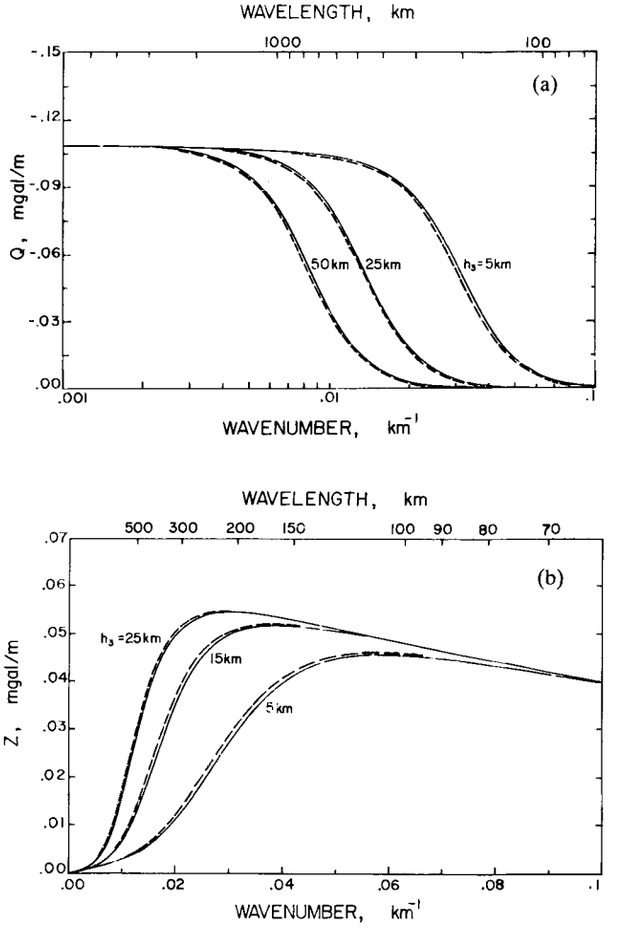

Figure 7. Comparison between the multilayered model (solid lines) and thin-plate model with the averaging scheme (dashed lines) for a three-layered plate as shown in Fig. 2 with parameters compiled in Table 1. (a) Isostatic response functions with thickness of the third layer varying from 5 to 50 km, $d = 0$ and $\rho_w = 0$. (b) Admittances with thickness of the third layer varying from 5 to 25 km.

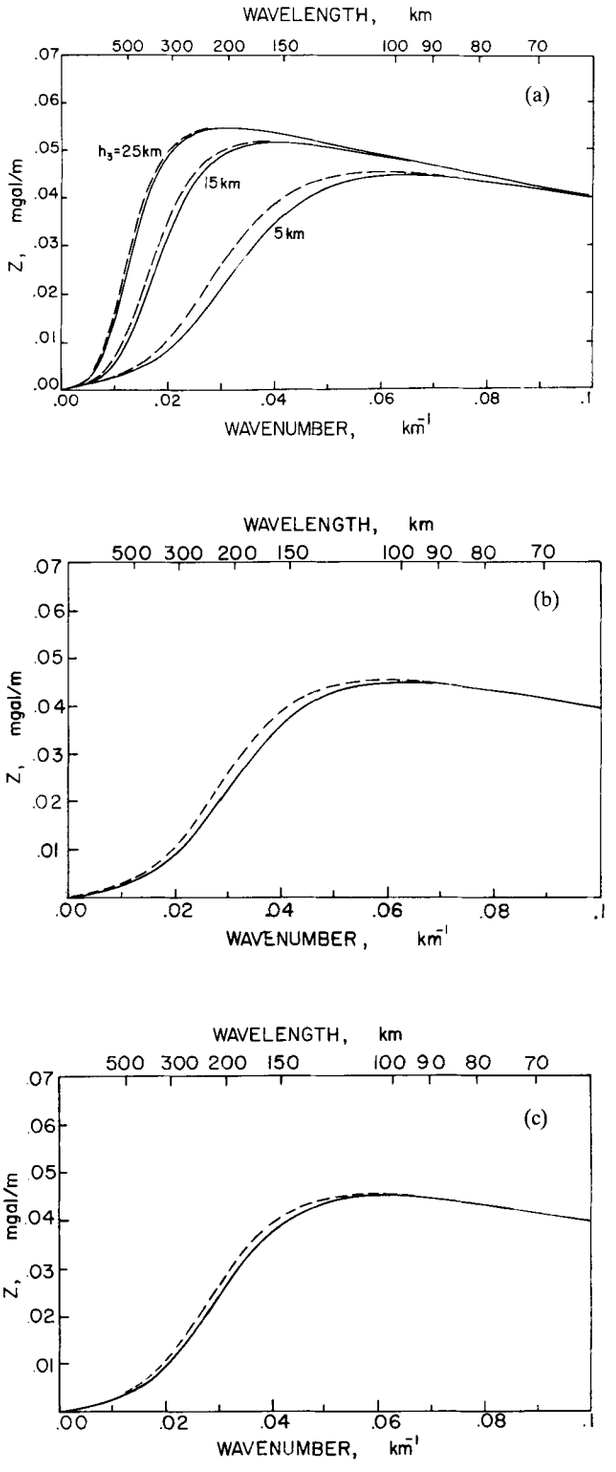

Figure 8. Admittances from the full theory (solid lines) and thin-plate approximation (dashed lines) with the averaging scheme for the large contrasts of the elastic moduli: (a) $E_1 = 10$ GPa, $E_2 = 50$ GPa and $E_3 = 100$ GPa and the thickness of the third layer varies from 5 km to 25 km. (b) $E_1 = 20$ GPa, $E_2 = 50$ GPa, $E_3 = 100$ GPa and $h_3 = 5$ km. (c) $E_1 = 30$ GPa, $E_2 = 60$ GPa, $E_3 = 100$ GPa and $h_3 = 5$ km. Other parameters are the same as shown in the Table 1.

thickness-averaged elastic moduli:

$$\bar{E} = \left(\sum_{j=1}^{n} h_j E_j\right) \Big/ \left(\sum_{j=1}^{n} h_j\right)$$
$$\bar{v} = \left(\sum_{j=1}^{n} h_j v_j\right) \Big/ \left(\sum_{j=1}^{n} h_j\right), \tag{29}$$

where E_j, v_j, h_j are the Young's modulus, Poisson's ratio and the thickness of the jth elastic layer, respectively, and n is the total number of the elastic layers (here $n = 3$).

The good agreement between the full theory and the thin-plate approximation for the three-layered plate model is illustrated for the isostatic response function (Fig. 7a) and the theoretical admittance (Fig. 7b). The agreement is also shown in Fig 4(a) and (b) (solid lines and chain lines) in comparison with observed admittance data. We have also tried other averaging schemes, but the above seems to provide the best agreement with the full theory. There seems to be no systematic way to find the effective elastic moduli to simulate the behaviour of the heterogeneous elastic plate with an arbitrary distribution of the elastic moduli using the thin-plate approximation. Our parametric study indicates that when the contrasts of elastic moduli at interfaces are up to or above one order of magnitude, the empirical averaging scheme above will introduce appreciable errors in the evaluation of the theoretical admittance by overestimating the effective flexural rigidity. It can be seen from the numerical examples in Fig. 8(a), (b) and (c) that the error introduced by the empirical averaging scheme is also a function of the plate thickness. Therefore, when the contrasts of the elastic moduli at interfaces are above one order of magnitude (which is probably unrealistically high) and the thickness of the upper mantle portion of the mechanical lithosphere is the same order as the thickness of the crust, we recommend that the full theory should be used. Otherwise, the thin-plate model using the above thickness-averaged physical properties would be quite adequate.

4.4 State of stress in a multilayered elastic plate subjected to flexure

The stress difference in a thin-plate model is linearly proportional to distance from the neutral axis and reaches maxima at the surface of the plate ($z = 0$) and at its base located at $z = H$ as sketched in Fig. 9(a). However, our current understanding of the rheological behaviour from experimental rock mechanics (Goetze & Evans 1979; Kirby 1980) indicates that such a linear distribution of stress within the lithosphere is physically unrealistic. As elaborated by McNutt & Menard (1982) and Watts *et al.* (1980), the mechanical response of the flexed lithosphere probably involves three separate regimes (Fig. 9b): a brittle regime in the uppermost, cool regions of the lithosphere where the rocks fail by movement along localized fractures, an elastic regime near the neutral plane and an underlying, ductile regime in which the rock deforms by thermally activated plastic flow.

Goetze & Evans (1979) formulated a scheme by which one can use the topography profile and constraints on failure behaviour from rock mechanics experiments to infer bounds

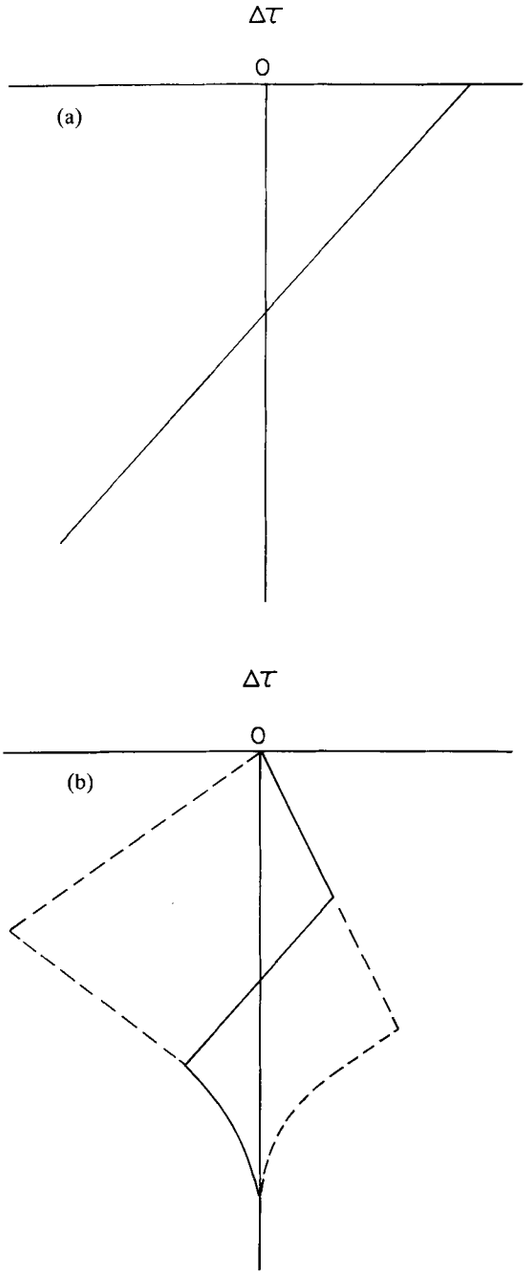

Figure 9. Principal stress difference versus depth in a cross-section of flexed lithosphere. (a) Homogeneous elastic plate model (stress difference varies linearly with depth). (b) Brittle-elastic-ductile model. Stress difference is bounded at the top of the plate by frictional sliding on favourably-oriented fractures, and at the base of the plate by plastic flow which depends on the strain rate and temperature.

on the state of stress within a flexed plate. Using this scheme, McNutt (1984) concluded that for plates bent to a relatively large curvature, the 'elastic thickness' estimated using previous approaches can be less than 75 per cent of the actual mechanical thickness. If the curvature is small, the discrepancy is negligible.

Goetze & Evans' (1979) scheme has been very useful principally because it is based solely on equilibrium considerations and hence the interpretation is independent of rheology. However, for precisely the same reason it provides no information on the displacement field or the deformation-induced gravity change.

Our technique can be used to compute the stress field in a multilayered plate. To illustrate the response of a heterogeneous plate with elastic modulus contrast, we first consider the three-layered model for an oceanic plate with parameters specified in Table 1. The stress field is a function of the wavelength of loading. We have chosen wave number $k = 0.02\ \mathrm{km}^{-1}$ in Fig. 10(a), (b) and (c) with a response representative of wavelengths within the 'compensated' band.

In response to a normal sinusoidal loading on the surface, σ_{xx} and σ_{zz} are out of phase with σ_{xz}. The latter vanishes at $kx = n\pi$ $(n = 0, 1, 2, \ldots)$ and therefore, at these locations, the principal stress difference is given by $\sigma_{xx} - \sigma_{zz}$. The two stress components at such locations are plotted in Fig. 10(a) and (b). (The computed results represent stress perturbation in a hydrostatically, pre-stressed medium. The ambient

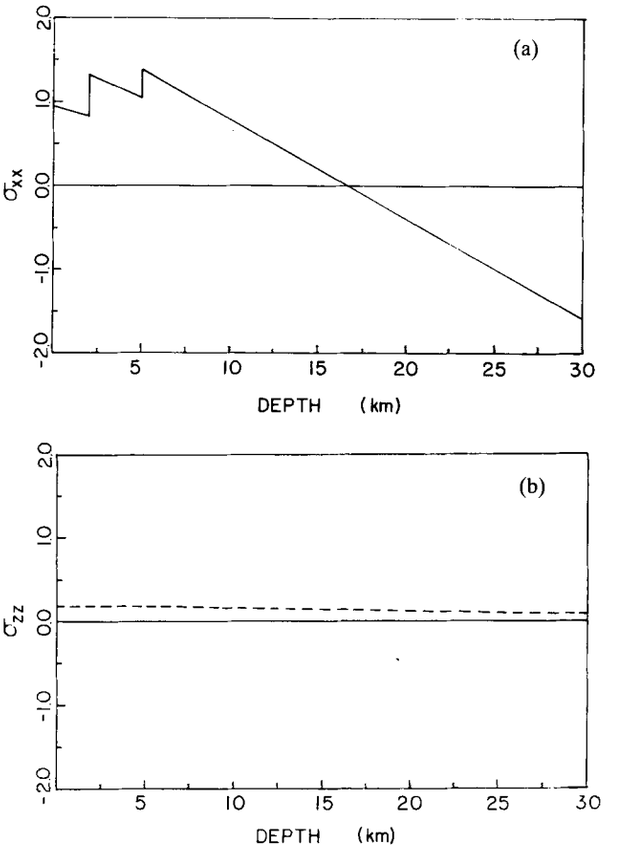

Figure 10. Distribution of stresses with depth for the wave number $k = 0.02\ \mathrm{km}^{-1}$. The stresses have been normalized by $10^5\ l$. l is the amplitude of loading. (a) horizontal stress σ_{xx} with $kx = 0$. (b) vertical stress σ_{zz} with $kx = 0$. (c) shear stress σ_{xz} with $kx = \pi/2$. The physical parameters for (a), (b) and (c) are compiled in Table 1 with the thickness of the third layer being 25 km. (d) horizontal stress σ_{xx} with $kx = 0$ for which the parameters are the same as those for (a), except that $E_1 = 10$ GPa, $E_2 = 50$ GPa and $E_3 = 100$ GPa are used.

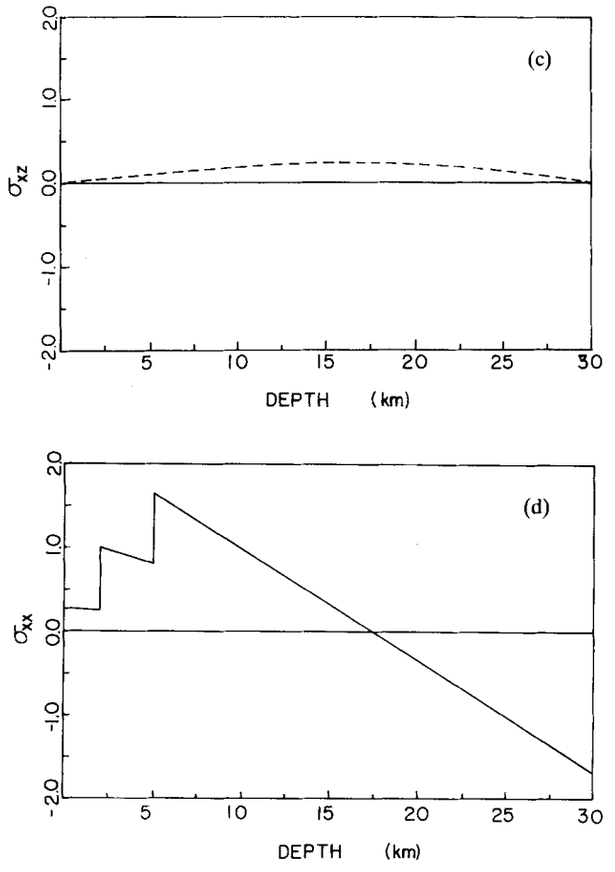

Figure 10. (c) and (d) (see previous page).

vertical stresses shown are given by the sum of σ_{zz} and the lithostatic pressure.) We have also plotted, in Fig. 10(c), the shear stress σ_{xz} for $kx = (n + \frac{1}{2})\pi$, at which locations both σ_{xx} and σ_{zz} vanish and the principal stress difference is given by $2\sigma_{xz}$.

It can be seen that in comparison with the other two stress components, the 'fibre stress' σ_{xx} is significantly larger in magnitude. Hence the depth variation of the differential stress is dominated by the variation of σ_{xx} as a function of z. Although σ_{xx} shows an essentially linear trend for the bottom layer, it undergoes discontinuous jumps at interfaces.

The behaviour is even more dramatic if we increase the contrast in Young's modulus to up to one order of magnitude (Fig. 10d). The fibre stress increases from a relatively low value to a maximum within the top two layers, and the trend is then reversed in a linear manner for the bottom layer. The differential stress distribution would therefore be analogous to that in a plate with extensive brittle faulting at the top and elastic behaviour below. Although we did not perform the computation, we would expect that if layers were introduced into the lower part of the plate with 'relaxed' elastic modulus values corresponding to anelastic behaviour due to thermally activated dislocation process in the upper mantle (Anderson & Minster 1980), the differential stress distribution would be similar to that schematically illustrated in Fig. 9(b).

Our computations demonstrate that the stress distribution in a heterogeneous elastic plate can be significantly different from that in a homogeneous plate. A similar conclusion was reached by Lambeck & Nakiboglu (1981) who specifically considered a parabolic and a circular load distribution on a three-layered thin-plate model. With suitable choices of elastic moduli as a function of depth, one may obtain stress distributions similar to those constrained by experimental rock mechanics results (Fig. 9b). However, our parametric study suggests that one would need to go to rather high contrast in elastic moduli to achieve this. Although laboratory studies show that the Young's modulus of a highly stressed or fractured rock can be somewhat less than that for a specimen subjected to small stress perturbation (Brace 1969) and that anelastic relaxation may cause difference between the 'dynamic' and 'static' moduli, an increase of Young's modulus within the crust ranging up to an order of magnitude or above is not very realistic.

In other words, if 'static' elastic moduli, as inferred from the 'dynamic' seismic moduli and from the anelastic properties, are relevant to a deformation process associated with lithospheric flexure, then our computations suggest that elastic deformation by itself is not sufficient to induce a stress distribution such as that shown schematically in Fig. 9(b). This implies that inelastic deformation plays an important role, and in order to fully characterize the internal displacement and the deformation-induced gravity change, one has to resort to an involved elastic–plastic analysis.

4.5 Subsurface loading

The estimates of flexural rigidity deduced from a linear transfer function with surface topographic loading are often lower than those obtained from analysis of individual features in continental regions. Forsyth (1981) has suggested that this discrepancy is caused by the neglect of density anomalies that load the plate within its interior or at its bottom. Based on the thin-plate theory, Louden & Forsyth (1982) and McNutt (1983) demonstrated that if loads are applied within the interior of the plate or at the bottom of the plate, the linear transfer function is dramatically different from the one with top-surface loading. In particular circumstances, the linear transfer function for sub-surface loading on a plate with high flexural rigidity may be similar to the one expected for a low-rigidity plate with top-surface loading. The multilayered model we developed here is applicable to such case with the sub-surface loading at the bottom of the plate. The boundary conditions for this case are:

$$\begin{aligned} &\sigma_{zz}(0) = 0 \\ &\sigma_{zx}(0) = 0 \\ &\sigma_{zx}(H) = 0 \\ &\sigma_{zz}(H) = -\rho_m g u_z(H) - \rho_l g l. \end{aligned} \tag{30}$$

The top surface of the plate is traction free. At the bottom of the plate, the shear stress is zero and the normal stress has two terms: buoyancy force due to the underlying fluid of density ρ_m and sub-surface loading due to a density anomaly ρ_l respectively. The displacement field can be determined with the propagator matrix technique, and the isostatic response function corresponding to the sub-surface loading

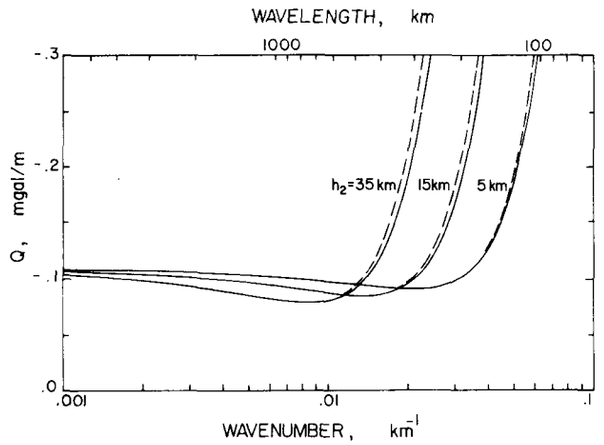

Figure 11. Theoretical isostatic response functions for a loading applied at the bottom of a two-layered elastic plate. Solid lines are from the full theory with the following parameters: $\rho_1 = 2600\,\mathrm{kg\,m^{-3}}$, $\rho_2 = \rho_m = 3400\,\mathrm{kg\,m^{-3}}$; $E_1 = 80$ GPa and $E_2 = 100$ GPa; $\upsilon_1 = 0.25$ and $\upsilon_2 = 0.36$; $h_1 = 5$ km and $h_2 = 5$–35 km. Dashed lines are from the thin-plate approximation using the averaging scheme to determine the flexure rigidity.

is easy to obtain from equations (15) and (25) in which the gravity effect of sub-surface load is included and the topography is the surface deflection caused by the sub-surface load. For purpose of illustration, we will considered a two-layered model [fig. 8 of McNutt's (1983) paper] and compare our result with equation 6 of McNutt's (1983) which is based on the thin-plate approximation. As shown in Fig. 11, the thin-plate approximation (dashed lines) is still very good for the sub-surface loading problem so long as the thickness-averaged elastic moduli are used. If we combine the loading effects from both top and bottom through the procedure described by Forsyth (1985), the expected isostatic response function for several different

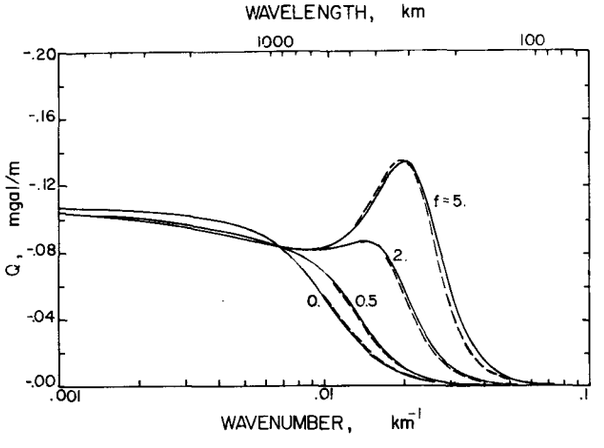

Figure 12. Theoretical isostatic response functions for loadings applied at both the top and the bottom of a two-layered elastic plate simultaneously. f is the ratio of the amplitude of the bottom load to the amplitude of the surface load. Solid lines are from the full theory with the following parameters: $\rho_1 = 2600\,\mathrm{kg\,m^{-3}}$ and $\rho_2 = \rho_m = 3400\,\mathrm{kg\,m^{-3}}$; $E_1 = 80$ GPa and $E_2 = 100$ GPa; $\upsilon_1 = 0.25$ and $\upsilon_2 = 0.36$; $h_1 = h_2 = 20$ km; $f = 0$–5. Dashed lines are from the thin-plate approximation using the thickness averaged elastic moduli.

ratios of bottom loading to top loading can be obtained as shown in Fig. 12 (solid lines). Again, a good agreement between the multi-layered model and thin-plate model (dashed lines) is arrived at if the thickness-averaged elastic moduli are used.

CONCLUSIONS

The deformation and gravity fields induced by the flexure of a 2-D multilayered elastic plate overlying an inviscid fluid have been calculated through the propagator matrix technique. The theoretical transfer function was evaluated and used to model the flexural response of the lithosphere under surface load. The model avoids some of the more restrictive assumptions previously used such as: (1) elastic incompressibility; (2) neglect of body force in the solid; (3) neglect of gravity change due to density perturbation within the lithospheric plate; (4) the thin-plate approximation; (5) neglect of elastic coupling among layers of different elastic moduli.

Our numerical results showed that the errors introduced by first three assumptions above can be neglected within the 'compensated' waveband. The thin-plate approximation is very good provided that flexural rigidity is evaluated using the thickness-averaged elastic moduli, unless the contrast in Young's modulus within the mechanical lithosphere is unexpectedly high (above an order of magnitude). If there is significant elastic coupling between the crust and the mantle, the incompressible thick-plate model will underestimate the elastic thickness, while at the same time it overestimates the extent of the mechanical lithosphere in the upper mantle. Although we have focused on the flexural response to surface loading, our preliminary calculations indicate that most of our conclusions regarding the surface loading response can be carried over to the sub-surface loading case. A heterogeneous plate comprising layers with different elastic moduli has a stress distribution appreciably different from that of a homogeneous, thin plate. By choosing a certain depth variation for the elastic moduli, it is possible to obtain stress distribution similar to that constrained by experimental results on failure behaviour and by equilibrium considerations. However, our calculations showed that unrealistically high contrast in elastic moduli would be required. Hence the inelastic deformation cannot be neglected and a complete elastic–plastic analysis is necessary.

ACKNOWLEDGMENTS

We have benefited from discussions with R. P. Comer and J. B. Walsh. Comments by R. P. Comer, D. M. Davis, and an anonymous reviewer on the manuscript have been very useful.

REFERENCES

Airy, G. B., 1855. On the computations of the effect of the attraction of the mountain masses as disturbing the apparent astronomical latitude of stations in geodetic surveys, *Phil. Trans. R. Soc. Lond.*, **145,** 101-104.

Anderson, D. L., & Minster, J. B., 1980. Seismic velocity, attenuation and rheology of the upper mantle, in *Source Mechanism and Earthquake Prediction,* Centre national de la Recherche Scientifique, Paris, 13–22.

Artyushkov, E. V., 1973. The stresses in the lithosphere caused by crustal thickness inhomogeneities, *J. geophys. Res.*, **78,** 7675–7708.
Banks, R. J., Parker, R. L. & Huestis, S. P., 1977. Isostatic compensation on a continental scale: local versus regional mechanisms, *Geophys. J. R. astr. Soc.*, **51,** 431–452.
Birch, F., 1966. Compressibility elastic constants, in *Handbook of Physical Constants,* S. P. Clarke ed, pp. 97–174.
Brace, W. F., 1969. Micromechanics in rock systems, *The Proceedings of the Southampton 1969 Civil Engineering Materials Conference,* ed. M. Te'eni, Wiley, 187–204.
Byerlee, J. D., 1978. Friction of rocks, *Pageoph,* **116,** 615–626.
Cathles, L. M., 1975. *The Viscosity of the Earth's Mantle,* Princeton University Press, Princeton, pp. 9–43.
Cazenave, A. & Dominh, K., 1984. Geoid heights over the Louisville ridge (South Pacific), *J. geophys. Res.*, **89,** 11171–11179.
Christensen, N. I., 1982. Seismic velocities, in *C. R. C. Handbook of Physical Properties of Rocks,* ed R. S. Carmichael, Vol. II, pp. 1–228.
Cochran, J. R., 1979. An analysis of isostasy in the world's oceans: 2. Mid-ocean ridge, *J. geophys. Res.*, **84,** 4713–4729.
Comer, R. P., 1983. Thick plate flexure, *Geophys. J. R. astr. Soc.*, **72,** 101–113.
Comer, R. P., 1986. Comments on: Thick-plate flexure re-examined' by Detlef Wolf, *Geophys. J. R. astr. Soc.*, **85,** 467–468.
Dahlen, F. A., 1981. Isostasy and the ambient state of stress in the oceanic lithosphere, *J. geophys. Res.*, **86,** 7801–7807.
Detrick,, R. S. & Watts, A. B., 1979. An analysis of isostasy in the world's oceans: 3. Aseismic ridges, *J. geophys. Res.*, **84,** 3637–3653.
Dorman, L. M. & Lewis, B. T. R., 1970. Experimental isostasy: 1, theory of the determination of the earth's isostatic response to a concentrated load, *J. geophys. Res.*, **75,** 3357–3365.
Farrell, W. E. 1972. Deformation of the earth by surface loads, *Rev. geophs. Space Phys.* **10,** 761–797.
Forsyth, D. W., 1985. Sub-surface loading and estimates of the flexural rigidity of continental lithosphere, *J. geophys. Res.*, **90,** 12623–12632.
Goetze, C. & Evans, B., 1979. Stress and temperature in the bending lithosphere as constrained by experimental rock mechanics, *Geophys. J. R. astr. Soc.*, **59,** 463–478.
Haskell, N. A., 1953. The dispersion of surface waves on multilayered media, *Bull. Seismol. Soc. Amer.*, **43,** 17–34.
Jachens, R. C. & Eaton, G. P., 1980. Geophysical observations of Kilauea volcano, Hawaii: 1, temporal gravity variations related to the 29 November 1975, M = 7.2 earthquake and associated summit collapse, *J. Volcanol. Geotherm. Res.*, **7,** 225–240.
Jachens, R. C. & Roberts, C. W., 1985. Temporal and areal gravity investigations at Long Valley Caldera, California, *J. geophys. Res.*, **90,** 11210–11218.
Kirby, S. H., 1980. Tectonic stresses in the lithosphere: constraints provided by the experimental deformation of rocks, *J. geophys. Res.*, **85,** 6353–6363.
Kogan, M. G. & Kostoglodov, V. V., 1981. Isostasy of fracture zones in the Atlantic Ocean, *J. geophys. Res.*, **86,** 9248–9258.
Lambeck, K. & Nakiboglu, S. M., 1980. Seamount loading and stress in the ocean lithosphere, *J. geophys. Res.*, **85,** 6403–6418.
Lambeck, K. & Nakiboglu, S. M., 1981. Seamount loading and stress in the ocean lithosphere 2. viscoelastic and elastic-viscoelastic models, *J. geophys. Res.*, **86,** 6961–6984.
Louden, K. E. & Forsyth, D. W., 1982. Crustal structure and isostatic compensation near the Kane fracture zone from topography and gravity measurements, 1, Spectral analysis approach, *Geophys. J. R. astr. Soc.*, **68,** 725–750.
Love, A. E. H., 1911. *Some Problems of Geodynamics,* Cambridge University Press, Cambridge, pp. 89–93.
McKenzie, D. P. & Bowin, C., 1976. The relationship between bathymetry and gravity in the Atlantic Ocean, *J. geophys. Res.*, **81,** 1903–1915.
McKenzie, D. P., 1977. Surface deformation, gravity anomalies and convection, *Geophys. J. R. astr. Soc.*, **48,** 211–238.
McNutt, M., 1979. Compensation of ocean topography: an application of the response function technique to the Surveyor area, *J. geophys. Res.*, **84,** 7589–7598.
McNutt, M., 1980. Implications of regional gravity for state of stress in the earth's crust and upper mantle, *J. geophys. Res.*, **85,** 6377–6396.
McNutt, M., 1983. Influence of plate subduction on isostatic compensation in northern California, *Tectonics*, **2,** 399–415.
McNutt, M., 1984. Lithospheric flexure and thermal anomalies, *J. geophys. Res.*, **89,** 11180–11194.
McNutt, M. & Menard, H. W., 1982. Constraints on yield strength in the oceanic lithosphere derived from observations of flexure, *Geophys. J. R. astr. Soc.*, **71,** 363–394.
Pratt, J. H., 1855, On the attraction of the Himalaya Mountains, and of the elevated regions beyond them, upon the plumb-line in India, *Phil. Trans. R. Soc. Lond.*, **145,** 53–100.
Rundle, J. B., 1978. Gravity changes and the Palmdale uplift, *Geophysical Res. Letters,* **5,** 41–44.
Rundle, J. B., 1982. Deformation, gravity and potential changes due to volcanic loading of the crust, *J. geophys. Res.*, **87,** 10729–10744.
Rundle, J. R., 1983. Correction to 'the deformation, gravity and potential changes due to volcanic loading of the crust', *J. geophys. Res.*, **88,** 10647–10652.
Savage, J. C., 1984. Local gravity anomalies produced by dislocation sources, *J. geophys. Res.*, **89,** 1945–1952.
Tamsett, D., 1984. An application of the response function technique to profiles of bathymetry and gravity in the gulf of Aden, *Geophys. J. R. astr. Soc.*, **78,** 349–369.
Vening Meinesz, F. A., 1941. Gravity over the Hawaiian Archipelago and over the Medeira area, *Proc. K. ned. Akad. Wet.*, **44,** 1–12.
Walcott, R. I., 1970. Flexure of the lithosphere at Hawaii, *Tectonophysics,* **9,** 435–446.
Walsh, J. B., 1982. Changes in gravity resulting from changes in topography, *J. geophys. Res.*, **87,** 6983–6988.
Walsh, J. B. & Rice, J. R., 1979. Local changes in gravity resulting from deformation, *J. geophys. Res.*, **84,** 165–170.
Ward, S. N., 1984. A note on lithospheric bending calculations, *Geophys. J. R. astr. Soc.*, **78,** 241–253.
Watts, A. B., 1978. An analysis of isostasy in the world's oceans: 1, Hawaiian-Emperor seamount chain, *J. geophys. Res.*, **83,** 5989–6004.
Watts, A. B., Bodine, J. H. & Steckler, M. S., 1980. Observations of flexure and the state of stress in the oceanic lithosphere, *J. geophys. Res.*, **85,** 6369–6376.
Wolf, D., 1985. Thick plate flexure re-examined, *Geophys. J. R. astr. Soc.*, **80,** 265–273.
Young, R. & Hill, Ian A., 1986. An estimate of the effective elastic thickness of the Cape Verde Rise, *J. geophys. Res.*, **91,** 4854–4866.

APPENDIX I

1 The list of non-zero elements of matrix M

$$M_{12} = -M_{43} = k$$

$$M_{13} = \frac{2(1+v)}{E}$$

$$M_{21} = -M_{34} = -\frac{kv}{(1-v)} \qquad \text{(I-1)}$$

$$M_{24} = \frac{(1+v)(1-2v)}{((1-v)E)}$$

$$M_{31} = \frac{k^2 E}{(1-v^2)}$$

$$M_{32} = M_{41} = k\rho g$$

2 Propagator matrix P

For the elastic plate subjected to a constant gravitation, there are four solutions (eigenvalues) of the characteristic equation of matrix **M**:

$$\lambda^4 - 2k^2\lambda^2 + k^4 - (kS)^2 = 0, \tag{I-2}$$

where

$$S = \frac{\rho g(1+\upsilon)}{E}\left[\frac{2(1-2\upsilon)}{1-\upsilon}\right]^{1/2}.$$

The four eigenvalues are:

$$\begin{aligned}\lambda_{1,2} &= \pm(k^2 + kS)^{1/2}\\ \lambda_{3,4} &= \pm(k^2 - kS)^{1/2}.\end{aligned} \tag{I-3}$$

Therefore the propagator matrix $\mathbf{P}[\![\exp[\mathbf{M}(k)(z-z_0)]]\!]$ can be expressed as a polynomial of the matrix **M**:

$$\begin{aligned}\mathbf{P} = &\frac{(\mathbf{M}-\lambda_2\mathbf{I})(\mathbf{M}-\lambda_3\mathbf{I})(\mathbf{M}-\lambda_4\mathbf{I})}{(\lambda_1-\lambda_2)(\lambda_1-\lambda_3)(\lambda_1-\lambda_4)}\exp[\lambda_1(z-z_0)]\\ &+\frac{(\mathbf{M}-\lambda_1\mathbf{I})(\mathbf{M}-\lambda_3\mathbf{I})(\mathbf{M}-\lambda_4\mathbf{I})}{(\lambda_2-\lambda_1)(\lambda_2-\lambda_3)(\lambda_2-\lambda_4)}\exp[\lambda_2(z-z_0)]\\ &+\frac{(\mathbf{M}-\lambda_1\mathbf{I})(\mathbf{M}-\lambda_2\mathbf{I})(\mathbf{M}-\lambda_4\mathbf{I})}{(\lambda_3-\lambda_1)(\lambda_3-\lambda_2)(\lambda_3-\lambda_4)}\exp[\lambda_3(z-z_0)]\\ &+\frac{(\mathbf{M}-\lambda_1\mathbf{I})(\mathbf{M}-\lambda_2\mathbf{I})(\mathbf{M}-\lambda_3\mathbf{I})}{(\lambda_4-\lambda_1)(\lambda_4-\lambda_2)(\lambda_4-\lambda_3)}\exp[\lambda_4(z-z_0)]\end{aligned} \tag{I-4}$$

under the assumption that material is homogeneous between z and z_0.

It can be observed from (I-3) that if gravitation is unimportant, i.e. $g=0$ in the solid or if the plate is incompressible ($\upsilon = 0.5$), there are only two eigenvalues (each of multiplicity two) of the matrix **M**:

$$\begin{aligned}\lambda_1 &= k\\ \lambda_2 &= -k.\end{aligned} \tag{I-5}$$

The matrix **P** then takes the form:

$$\begin{aligned}\mathbf{P} = &\left\{\frac{1}{(\lambda_1-\lambda_2)^2}+\left[\frac{-2}{(\lambda_1-\lambda_2)^3}+\frac{(z-z_0)}{(\lambda_1-\lambda_2)^2}\right]\right.\\ &\left.\times(\mathbf{M}-\lambda_1\mathbf{I})\right\}(\mathbf{M}-\lambda_2\mathbf{I})^2\exp[\lambda_1(z-z_0)]\\ &+\left\{\frac{1}{(\lambda_2-\lambda_1)^2}+\left[\frac{-2}{(\lambda_2-\lambda_1)^3}\right.\right.\\ &\left.\left.+\frac{(z-z_0)}{(\lambda_2-\lambda_1)^2}\right](\mathbf{M}-\lambda_2\mathbf{I})\right\}(\mathbf{M}-\lambda_1\mathbf{I})^2\exp[\lambda_2(z-z_0)].\end{aligned} \tag{I-6}$$

3 Some equations used in this paper

According to Hamilton–Cayley theorem, every square matrix **M** satisfies its characteristic equation. Therefore we have from (I-2):

$$\mathbf{M}^4 - 2k^2\mathbf{M}^2 + [k^4 - (kS)^2]\mathbf{I} = 0. \tag{I-7}$$

Multiplication of (I-7) on the right by $\mathbf{V}(z)$ and from (4), we get

$$\nabla^2[\mathbf{V}(z)\exp(ikx)] = (\mathbf{M}^2 - k^2\mathbf{I})\mathbf{V}(z)\exp(ikx) \tag{I-8}$$

and

$$\nabla^4[\mathbf{V}(z)\exp(ikx)] = (kS)^2\mathbf{V}(z)\exp(ikx). \tag{I-9}$$

(I-9) shows that for a compressible elastic medium under the action of a body force, the stress and displacements are not biharmonic. If $g \neq 0$ in the solid or if $\upsilon = 0.5$ (incompressible case), the stress and displacement fields satisfy the biharmonic equation. For the special case that $g = 0$ in the solid, we can use (I-8) to obtain:

$$\nabla^2(iu_x\exp(ikx)) = \frac{k}{(1-\upsilon)}\left[iku_x + \frac{(1+\upsilon)}{E}\tau_{zz}\right]\exp(ikx). \tag{I-10}$$

Using Hooke's law to relate τ_{zz} to the displacement gradients, we have:

$$\nabla\cdot\mathbf{U} = \frac{(1-2\upsilon)}{k}\nabla^2[iu_x\exp(ikx)] \tag{I-11}$$

APPENDIX II

The derivation of equation (14)

From Fig. 1, the distribution of the density for the multilayered model is:

$$\begin{aligned}\rho(z) = &\rho_w\bar{U}(z+d) + (\rho_1-\rho_w)\bar{U}(z)\\ &+\sum_{j=1}^{n-1}(\rho_{j+1}-\rho_j)\bar{U}(z-z_j)\\ &+(\rho_m-\rho_n)\bar{U}(z-H)\end{aligned} \tag{II-1}$$

in the absence of the deformation. We assume the density of the first layer ρ_1 to be equal to the density of the loading material ρ_b, and $\bar{U}$ is the Heaviside step function.

The derivative of (II-1) with respect to z has form

$$\begin{aligned}\rho'(z) = &\rho_w\delta(z+d) + (\rho_1-\rho_w)\delta(z)\\ &+\sum_{j=1}^{n-1}(\rho_{j+1}-\rho_j)\delta(z-z_j) + (\rho_m-\rho_n)\delta(z-H)\end{aligned} \tag{II-2}$$

where δ is the Dirac delta.

The Bouguer component of the gravity potential caused by the first term of (12) can be obtained through (11) and (II-2):

$$\begin{aligned}\phi_1^B = G\int\int_{-\infty}^{+\infty}&\left[\frac{-(\rho_1-\rho_w)\Delta}{R_0}+\sum_{j=1}^{n-1}\frac{(\rho_{j+1}-\rho_j)u_z(z_j)}{R_j}\right.\\ &\left.+\frac{(\rho_m-\rho_n)u_z(H)}{R_n}\right]\exp(ikx)\,dx\,dy,\end{aligned} \tag{II-3}$$

where R_j is the distance between the field point and the source point which is on the j-th boundary surface S_j. The static deformation at sea surface is considered to be zero, and Δ is the topography on the seafloor as defined in equation (8). $u_z(z_j)$ is the vertical deformation at z_j. To arrive at the above, we have used the result that:

$$\int_{-\infty}^{+\infty} f(z)\,\delta(z-a)\,dz = f(a). \tag{II-4}$$

The Bouguer component of the vertical component

gravity change is:

$$\delta g^{B} = -\partial\phi_1^{B}/\partial z'$$

$$= G\iint_{-\infty}^{+\infty}\left[\frac{-z'(\rho_1-\rho_w)\Delta}{R_0^{3/2}} + \sum_{j=1}^{n-1}\frac{(z'-z_j)(\rho_{j+1}-\rho_j)u_z(z_j)}{R_j^{3/2}}\right.$$

$$\left. + \frac{(z'-H)(\rho_m-\rho_n)u_z(H)}{R_n^{3/2}}\right]\exp(ikx)\,dx\,dy. \qquad \text{(II-5)}$$

By using the integral:

$$\iint_{-\infty}^{+\infty}\frac{(z'-z_j)\exp(ikx)\,dx\,dy}{R_j^{3/2}}$$

$$= -2\pi\exp[k(z'-z_j)]\exp(ikx') \qquad (z'-z_j<0) \quad \text{(II-6)}$$

where $z'-z_j<0$ is satisfied for $z_j>0$ with field point at sea surface, equation (II-5) can be written in a closed form with the field point at $z'=-d$ of the sea surface, which is equation (13) with Z^{B} given by equation (14).